Article ID:1002-1175(2011)02-0161-08

Dissociative photoionization of methylbutenol: experimental and computational investigations*

SUN Yue[1], ZHAO Yu-Jie[1], FANG Wen-Zheng[1], SUN Jin-Da[1], SHAN Xiao-Bin[1], LIU Fu-Yi[1], SHENG Liu-Si[1†], WANG Zhen-Ya[1,2]

(1 *National Synchrotron Radiation Laboratory, School of Nuclear Science and Technology, University of Science and Technology of China, Hefei* 230029, *China*; 2 *Laboratory of Environmental Spectroscopy, Anhui Institute of Optics and Fine Mechanics, Chinese Academy of Sciences, Hefei* 230031, *China*)

(Received 20 May 2010; Revised 10 June 2010)

Sun Y, Zhao Y J, Fang W Z, et al. Dissociative photoionization of methylbutenal: experimental and computational investigations [J]. Journal of the Graduate School of the Chinese Academy of Sciences, 2011, 28(2):161 - 168.

Abstract Vacuum ultraviolet (VUV) dissociative photoionization of methylbutenol ($C_5H_{10}O$) in 9.0 ~ 15.5 eV was investigated with photoionization mass spectrometry using synchrotron radiation (SR). The ionization energy of $C_5H_{10}O$ and the appearance energies for the main fragment ions were determined with photoionization efficiency curves. The photodissociation mechanisms of methylbutenol were discussed based on comparison of our experimental results with those predicted by the quantum-chemical calculations. The dissociation channels may be divided into two types: the direct bond cleavage in $C_5H_{10}O^+$ and the reactions involving transition states. Transition states and intermediates for $C_4H_5^+$ and $C_3H_5^+$ were determined, and the reaction barriers were in agreement with the experimental dissociation energies.

Key words methylbutenol, photoionization and photodissociation, synchrotron radiation, G3B3 calculation

CLC O641

Methylbutenol (MBO, 2-Methyl-3-buten-2-ol, $CH_3—C(OH)(CH_3)—CH=CH_2$) is mainly used as starting material or intermediate in the synthesis of drugs, vitamins, and flavoring agents etc. Minor amounts are used as attractant in bark traps [1]. MBO is also an important biogenic hydrocarbon emitted in large quantities by pine forests (about 9.6 T_g per year) [2-4], and its oxidation causes an increasing in ozone, formaldehyde, acetone, and consequently hydrogen radical production (PHO_x) [5-8].

The ionization energy of the MBO molecule was estimated in 1979 under electron impact and chemical ionization conditions [9]. The mechanism for removal of methyl from the MBO ion was investigated using isotopic labeling, metastable ion, and field ionization kinetics (FIK) studies in 1981 [10]. Recently, the

* Supported by the National Natural Science Foundation of China (10675112), 973 fund of Chinese Ministry of Science and Technology (2010CB934504), and the Knowledge Innovation Foundation of the Chinese Academy of Sciences (KJCX2-YW-N24)

† Corresponding author, E-mail: lssheng@ustc.edu.cn

ultraviolet absorption spectrum of MBO between 210 nm and 300 nm was measured using a 50 cm-long absorption cell, a D2 lamp, and a diode array spectrometer [11]. However, the dissociative photoionization of MBO ($C_5H_{10}O$) at higher ionization energies is little investigated, either experimentally or theoretically, and the mechanism for the dissociative photoionization is unclear until now.

In order to explore the dissociative photoionization of $C_5H_{10}O$ experimentally and theoretically, the experimental measurements with a photoionization mass spectrometer coupled to a synchrotron radiation as an ionization source were performed, and the calculations of total energies using the G3B3 method [12-13] were carried out [14]. The IE of $C_5H_{10}O$ and AEs of its fragment ions were measured experimentally and predicted theoretically. The dissociative photoionization channels are proposed on the basis of the experimental and calculated dissociation energies and some transition-state energies.

1 Experimental set-up

Our experimental apparatus has been described previously [15-16]. We performed photoionization mass spectrometry (PIMS) measurements on the atomic and molecular physics beamline with the supersonic expansion molecular beam/a reflectron time-of-flight mass spectrometer (RTOFMS) system at the National Synchrotron Radiation Laboratory (NSRL) in Hefei, China. The produced ions were detected with RTOFMS mounted in a direction perpendicular to the plane defined by molecular and photon beams. Photon energies in the region 7.5 ~22.5 eV with a resolving power of 5000 at 15.9 eV and a photon flux of 10^{12} photons/s were selected with a grazing-incidence SGM monochromator employing a 370 lines/mm grating and a slit width of 80 μm. The monochromatic synchrotron radiation was focused by a toroidal mirror the photoionization chamber. A rare-gas harmonic filter was inserted into the beamline to overcome higher-order harmonics contamination in the energy range between 7.5 eV and 21.5 eV. In this experiment, the monochromator was calibrated with the known ionization energies and special ionization spectra of the inert gases (Ne, Ar, and Xe).

MBO was obtained from J&K Chemical Ltd, Europe, and used without additional purification. In this experiment, Ar (purity 99.99%) was used as the carrier gas and the stagnation pressure was in the range of 1.2 ~1.6 atm. Ar was also used as gas filter medium and the pressure in the gas chamber was 600 Pa. Before the experiments, the pressure in the ionization chamber was about 5.1×10^{-5} Pa, and it was 3.0×10^{-3} Pa when the sample was introduced. The PIE curves were measured while the monochromator was scanned with a photon energy increment of 30 meV. The data acquisition time for each point was 30 ~40 s depending on ion abundance.

2 Computational details

In our calculations, density functional theory (DFT) [17-18] was employed with the B3LYP functional. The 6-31G (d) basis set was used in all the geometry optimization calculations for the parent molecule, its fragments, and the transition states. The vibrational freguency analyses for all the species were performed at the B3LYP/6-31G (d) level to characterize minima or a transition states in the potential energy surfaces (PES). In addition, the G3B3 method [12-13] was used to obtain the G3B3 energies and the thermochemical parameters, such as ionization energy of MBO, appearance energies for its fragment ions, and dissociation energies. All the calculations were carried out using the Gaussian 03 program [14].

3 Results and discussion

3.1 Experimental results

Figure. 1 shows the photoionization mass spectroscopy of $C_5H_{10}O$ excited at 15.5 eV. The parent ion

$C_5H_{10}O^+$ (m/z = 86), the five major fragment ions, $C_4H_7O^+$, $C_3H_7O^+$, $C_2H_3O^+$, $C_3H_7^+$, and $C_3H_5^+$, and the four minor fragment ions, $C_5H_9^+$, $C_3H_6O^+$, $C_4H_5^+$, and CH_3O^+, are observed. As shown in the figure, the number of the parent ion $C_5H_{10}O^+$ is rare, which indicates the parent ion is unstable. The signal of the fragment ion m/z = 43 is the strongest among all the fragment ions when the $C_5H_{10}O$ is excited at the photon energy of 15.5 eV.

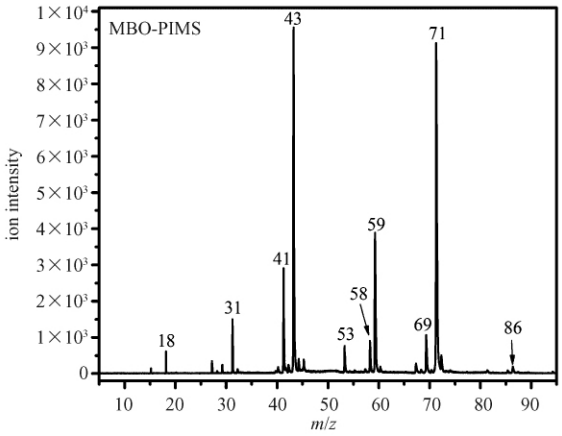

Fig. 1　Photoionization mass spectroscopy of MBO at 15.5eV

The photoionization efficiency (PIE) curves of $C_5H_{10}O^+$ and some important fragment ions, such as $C_4H_7O^+$, $C_3H_7O^+$, $C_2H_3O^+$, $C_3H_7^+$, $C_3H_5^+$, $C_5H_9^+$, $C_3H_6O^+$, $C_4H_5^+$, and CH_3O^+ from their respective appearance onsets to 15.5 eV were recorded at a scan step of 30 meV and normalized with respect to the photon flux. The PIE curves near the threshold region of the parent molecular ion $C_5H_{10}O^+$ and some fragment ions, $C_4H_7O^+$, $C_2H_3O^+$, and $C_3H_7^+$, are shown in Figs. 2 and 3. As shown in Fig. 3, the strongest peak (m/z = 43) is contributed by both $C_2H_3O^+$ and $C_3H_7^+$. In the study of VUV dissociative photoionization of $C_5H_{10}O$ in the energy region 9.0 ~ 15.5 eV, the IE of $C_5H_{10}O$ and the AEs of the fragment ions can be obtained directly by scanning the photon energy of the monochromatic SR.

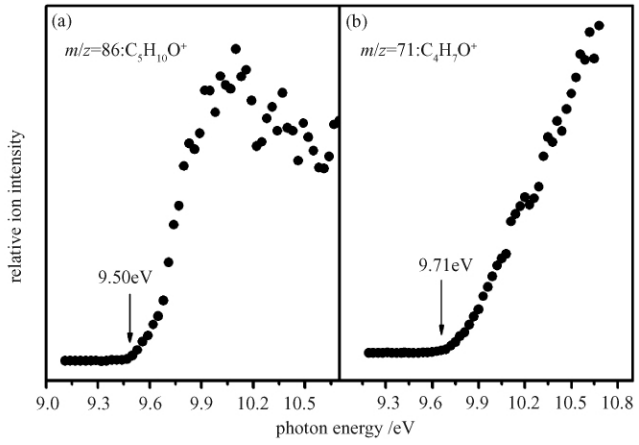

Fig. 2　Photoionization efficiency curve of $C_5H_{10}O^+$ and $C_4H_7O^+$

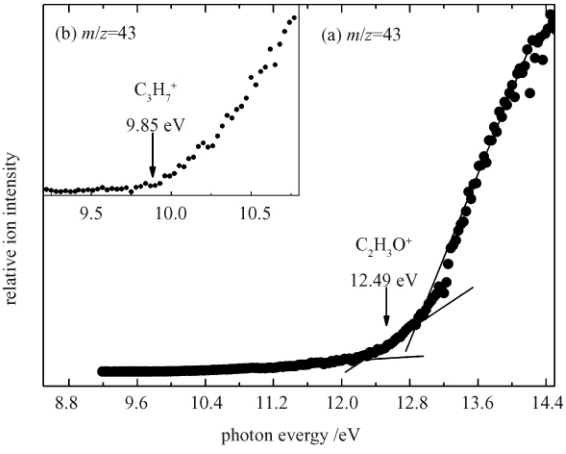

Fig. 3　Photoionization efficiency curves for m/z = 43 ions: (a) $C_2H_3O^+$ and (b) $C_3H_7^+$ (×5)

The PIE curves near the threshold regions of $C_5H_{10}O^+$ (Fig. 2(a)), $C_4H_7O^+$ (Fig. 2(b)), $C_2H_3O^+$ (Fig. 3(a)), and $C_3H_7^+$ (Fig. 3(b)) serve to determine the IE for parent ion and AE for each fragment ion. The experimental IE of the $C_5H_{10}O$ parent molecule is (9.50 ± 0.01) eV. For the fragment ions, two approaches were used to determine their appearance energies [19]. For ion signals that increase with photon energy, the AE was determined from the intersection of the baseline and the gradually rising line, as shown in Fig. 2(b) for $C_4H_7O^+$ ((9.71 ± 0.03) eV) and in Fig. 3(b) for $C_3H_7^+$ ((9.85 ± 0.06) eV). If the ion signal rises abruptly but with a gradual and slow slope near the threshold, the AE was determined as the midpoint of the two intersects among the baseline, the slowly rising line and the rapidly rising line, as shown

in Fig. 3(a) for $C_2H_3O^+$ ((12.49 ± 0.13) eV). For the PIE curves of all ions, the measurements have been repeated for three times and the mean threshold values plus error are evaluated.

The IE of MBO and the AE values of the observed fragment ions in our work are listed in Table 1. From comparison with the experimental IE value of MBO and with the reported value [9], it is obvious that the first measurements of AE values for all observed fragment ions are represented in this article. In general, the fragment ion is formed by ionization of the parent molecule followed by the spontaneous dissociation of the primary parent ion, which is referred to dissociation ionization. The experimental dissociation energy E_d is evaluated empirically by subtracting IE of the parent molecule from its AE, E_d = AE − IE, where E_d is the dissociation energy, AE is the appearance energy for fragment ion, and IE is the ionization energy of parent molecule. Taking the case of $C_4H_7O^+$, the IE of $C_5H_{10}O$ is (9.50 ± 0.01) eV and the AE of $C_4H_7O^+$ is (9.71 ± 0.03) eV. Consequently, the experimental dissociation energy $E_d(C_4H_7O^+—CH_3)$ is (0.21 ± 0.06) eV. The experimental IE of $C_5H_{10}O$, AE for each fragment ion, and E_d are listed in Table 1, along with some experimental dissociation energies and possible dissociation channels of $C_5H_{10}O$.

3.2 Calculation results

The geometries of MBO, neutral fragment radicals, and their corresponding ions were optimized, and the equilibrium geometries of MBO and its parent ion are shown in Fig. 4(a) and Fig. 4(b). By aid of the calculated results, the mechanism of dissociative photoionization of MBO will be explored and discussed.

Ionization energy (IE) of each molecule is defined as the energy required for removal of remove an electron from a molecule, calculated as the energy difference between the cation and the neutral molecule. The ionization energy of MBO is calculated using the following equation

$$IE(C_5H_{10}O) = E_0(G3B3)(C_5H_{10}O^+) - E_0(G3B3)(C_5H_{10}O). \quad (1)$$

This calculated value of adiabatic ionization energy of MBO, 9.70eV, is in agreement with experimental value of (9.50 ± 0.01) eV, which is shown in Table 1.

For the possible dissociation channel $C_5H_{10}O \rightarrow C_4H_7O^+ + CH_3$, the AE of $C_4H_7O^+$ is calculated by

$$AE(G3B3) = E_0(G3B3)(C_4H_7O^+) + E_0(G3B3)(CH_3) - E_0(G3B3)(C_5H_{10}O). \quad (2)$$

The calculated AE of $C_4H_7O^+$, 9.71eV, is the same as the experimental value of (9.71 ± 0.03) eV. Comparisons of the calculated results with the experimental values give additional support to the use of the G3B3 method in the present context as shown below. The dissociation energy can be calculated by

$$E_d(G3B3) = E_0(G3B3)(C_4H_7O^+) + E_0(G3B3)(CH_3) - E_0(G3B3)(C_5H_{10}O^+). \quad (3)$$

The appearance energies of other fragment ions and some dissociation energies of other possible dissociation channels are calculated in similar ways. The calculated IE of MBO, AE for each fragmental ion, and E_d for each possible dissociation channel are listed in Table 1.

3.3 Discussion of dissociation mechanisms

The $C_5H_{10}O^+$ molecular ion can be generated directly by a single-photon ionization of the VUV synchrotron radiation. The $C_5H_{10}O^+$ dissociation reactions may be simply divided into two types: simple bond cleavage reactions and indirect bond cleavage reactions involving transition states and intermediates [9-20].

$C_5H_9^+$ is generated directly from the parent molecular ion by OH-elimination (Channel 1) (Fig. 4(b)). $C_4H_7O^+$ is produced by CH_3-elimination from parent molecular ion $C_5H_{10}O^+$, and the possible dissociation channel(channel 2) is $C_5H_{10}O^+ \rightarrow C_4H_7O^+ + CH_3$. The C3—C5 bond length in neutral $C_5H_{10}O$ is 1.540×10^{-8} cm, but it is as long as 1.736×10^{-8} cm in $C_5H_{10}O^+$ (in Fig. 4(a),(b)). It means that the C3—C5 bond in $C_5H_{10}O^+$ will be broken and a more stable geometry is formed [10]. On the other hand, the calculated dissociation energy is very small (0.01eV). In conclusion, the dissociation channel $C_5H_{10}O^+ \rightarrow C_4H_7O^+ +$

CH_3 may involve direct cleavage of C3—C5 bond by the single photoionization of $C_5H_{10}O$. Moreover, the signal of $C_4H_7O^+$ is the second biggest one in intensity in the photoionization mass spectroscopy of $C_5H_{10}O$ (Fig. 1), which is slightly smaller in intensity than the signal of $m/z = 43$.

Table 1　The calculated, experimental, and reported values of the ionization energy (IE), appearance energy (AE), and dissociation energy (E_d) of MBO

ions	IE or AE (G3B3) /eV	IE or AE (Exp.) /eV	IE or AE (reported) /eV	possible dissociation channels	E_d (G3B3) /eV	E_d (Exp.) /eV
$C_5H_{10}O^+$	9.70	9.50 ± 0.01	9.90 (PE) [9]	–	–	–
$C_5H_9^+$	10.65	10.70 ± 0.03	–	$C_5H_9^+ + OH$ (1)	0.95	1.20 ± 0.06
$C_4H_7O^+$	9.71	9.71 ± 0.03	–	$C_4H_7O^+ + CH_3$ (2)	0.01	0.21 ± 0.06
$C_3H_7O^+$	10.34	10.36 ± 0.03	–	$C_3H_7O^+ + C_2H_3$ (3)	0.64	0.86 ± 0.06
$C_4H_5^+$	11.86	12.37 ± 0.06	–	$C_4H_5^+ + CH_3 + H_2O$ (4)	2.17	2.87 ± 0.12
$C_3H_5^+$	12.84	13.03 ± 0.05	–	$C_3H_5^+ + C_2H_3 + H_2O$ (5)	3.10	3.53 ± 0.10
$C_3H_6O^+$	9.76	9.66 ± 0.02	–	$C_3H_6O^+ + C_2H_4$ (6)	0.06	0.16 ± 0.04
$C_2H_3O^+$	12.69	12.49 ± 0.13	–	$C_2H_3O^+ + C_2H_4 + CH_3$ (7)	2.99	2.99 ± 0.26
CH_3O^+	12.99	12.48 ± 0.15	–	$CH_3O^+ + C_2H_3 + C_2H_4$ (8)	3.29	2.98 ± 0.30
$C_3H_7^+$	10.74	9.85 ± 0.06	–	$C_3H_7^+ + CO + CH_3$ (9)	1.04	0.35 ± 0.12

Similarly, $C_3H_7O^+$ is formed from the parent molecular ion $C_5H_{10}O^+$ by cleavage of C2—C3 bond, and the possible dissociation channel is $C_5H_{10}O^+ \rightarrow C_3H_7O^+ + C_2H_3$. As seen in Fig. 4(a) and Fig. 4(b), the C2—C3 bond length is 1.519×10^{-8} cm in neutral $C_5H_{10}O$ which decreases to 1.472×10^{-8} cm in $C_5H_{10}O^+$. Therefore, the breaking of the C2—C3 bond would be much more difficult than that of the C3—C5 bond. Consequently, the signal of $C_3H_7O^+$ is the third biggest one, but it is only half of the signal of $C_4H_7O^+$. On the basis of our calculated E_d valuas listed in Table 1, one can find that the experimental E_d values for channels 1 ~ 3 are close to the E_d (G3B3) values, respectively, reflecting that our prediction of the reaction channels 1 ~ 3 is reasonable.

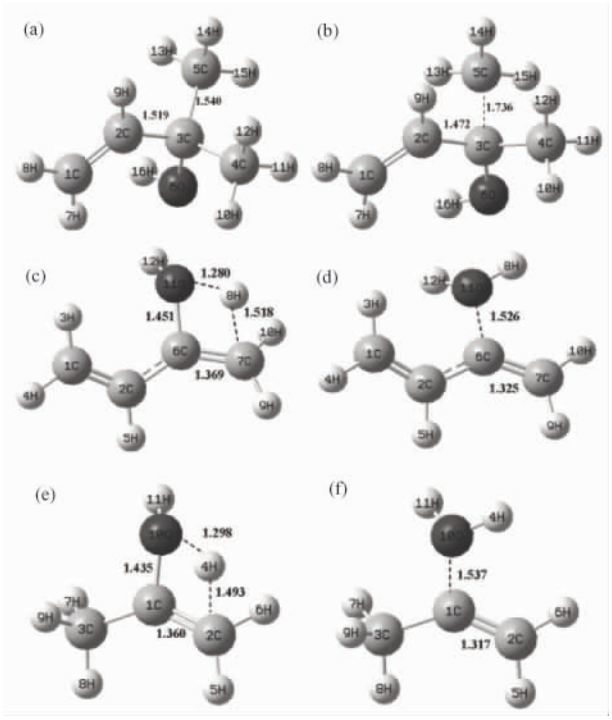

图 4　Equilibrium geometries of (a) $C_5H_{10}O$, (b) $C_5H_{10}O^+$, (c) TS1, (d) IM1, (e) TS2, and (f) IM2 at the B3LYP/6-31G(d) level

Channels 4 ~ 9 can indirectly generate the products by aid of geometrical rearrangement and adjustment, transition states, and intermediates. Relative energies of reactant, transition state, intermediate, and products and the possible mechanism for the dissociation channel $C_5H_{10}O^+ \rightarrow C_4H_5^+ + CH_3 + H_2O$ (channel 4) are listed in Table 2 and shown in Fig. 5, respectively. The $C_4H_5^+$, CH_3, and H_2O products are formed finally via a transition state TS1 (Fig. 4(c)) and an intermediate IM1 (Fig. 4(d)). It is found in Fig. 5 that the relative energy

of $C_4H_7O^+$ (TS1) + CH_3 is 2.98eV, which is larger than the calculated value of 2.17eV for the dissociation energy. So the reaction barrier of this dissociation channel is 2.98eV, which is almost identical to the experimental value of dissociation energy for this dissociation channel (2.87eV). Similarly, relative energies of the possible mechanism for the dissociation channel $C_5H_{10}O^+ \rightarrow C_3H_5^+ + C_2H_3 + H_2O$ (channel 5) are listed in Table 2 and shown in Fig. 6. The geometues of the transition state TS2 and intermediate IM2 are shown in Fig. 4(e) and Fig. 4(f). Furthermore, the calculated reaction barrier (V(G3B3)) for this reaction (3.63eV) is in good agreement with the experimental E_d value (3.53eV).

Table 2 Energies of various dissociation channels $C_5H_{10}O^+ \rightarrow C_4H_5^+ + CH_3 + H_2O$ and $C_5H_{10}O^+ \rightarrow C_3H_5^+ + H_2O + C_2H_3$

	E_0(G3B3) (hartree)	relative energy E_d(G3B3)/eV	relative energy E_d(Exp.)/eV
$C_5H_{10}O^+$	-271.167986	-	-
$C_4H_7O^+ + CH_3$	-271.167708	0.01	0.21
$C_4H_7O^+$ (TS1) + CH_3	-271.058606	2.98 V(G3B3)	-
$C_4H_7O^+$ (IM1) + CH_3	-271.117198	1.38	-
$C_4H_5^+ + CH_3 + H_2O$	-271.088375	2.17	2.87
$C_3H_7O^+ + C_2H_3$	-271.144324	0.64	0.86
$C_3H_7O^+$ (TS2) + C_2H_3	-271.034610	3.63 V(G3B3)	-
$C_3H_7O^+$ (IM2) + C_2H_3	-271.098318	1.90	-
$C_3H_5^+ + C_2H_3 + H_2O$	-271.054152	3.10	3.53

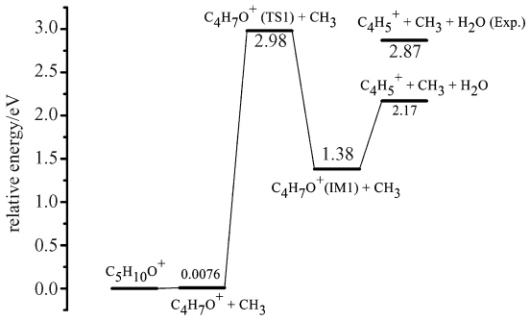

Fig. 5 The calculated relative energies of the species for the dissociation channel $C_5H_{10}O^+ \rightarrow C_4H_5^+ + CH_3 + H_2O$ at the G3B3 level

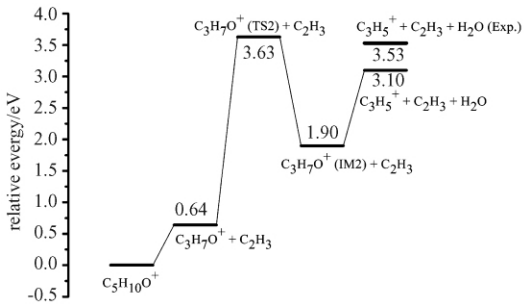

Fig. 6 The calculated relative energies of the species for the dissociation channel $C_5H_{10}O^+ \rightarrow C_3H_5^+ + C_2H_3 + H_2O$ at the G3B3 level

$C_3H_6O^+$, $C_2H_3O^+$, and CH_3O^+ may be generated by elimination of C_2H_4 from $C_5H_{10}O^+$, $C_4H_7O^+$ [10], and $C_3H_7O^+$, respectively. The $C_3H_7^+$ product is formed after CO is eliminated from $C_4H_7O^+$ [10]. As shown in Fig. 1, the ion intensity of $m/z = 43$ in our measured mass spectra is the biggest one, indicating that under the single photoionization condition the channels leading to the $m/z = 43$ ion is the important dissociative channels of $C_5H_{10}O$, which is different from the mass spectroscopy on the NIST (National Institute of Standards and Technology) Chemistry WebBook [21]. However, there are two onesets in the PIE curve of $m/z = 43$ ion. According to the prediction of Zwinselman et. al., the possible dissociation channels for the $m/z = 43$ ion are $C_5H_{10}O^+ \rightarrow C_2H_3O^+ + C_2H_4 + CH_3$ (channel 7) and $C_5H_{10}O^+ \rightarrow C_3H_7^+ + CO + CH_3$ (channel 9) [10]. For $C_2H_3O^+$, the experimental E_d value is the same as the calculated value (2.99eV), but the experimental E_d

value for $C_3H_7^+$ is 0.35eV, which deviates from the calculated value of 1.04eV. Therefore, the $C_2H_3O^+$ ion contributes more to the intensity of $m/z = 43$, which is also in line with the prediction of Zwinselman et. al. [10]. As shown in Table 1, the experimental E_d for channels 6 and 7 are in good agreement with the calculated E_d (G3B3) values, respectively. However, the experimental E_d data for channels 8 and 9 are smaller than the calculated E_d (G3B3) values, implying that in future studies we should consider not only the calculated dissociation energies but also some different transition states with specific barriers for understanding the dissociation mechanism of MBO molecule.

4 Conclusion

Photoionization mass spectrometry (PIMS) with synchrotron radiation as an ionization source has been used to study the dissociative photoionization of $C_5H_{10}O$ to form fragment ions $C_4H_7O^+$, $C_5H_9^+$, $C_3H_7O^+$, $C_3H_6O^+$, $C_4H_5^+$, $C_2H_3O^+$, $C_3H_7^+$, $C_3H_5^+$, and CH_3O^+. The experimental dissociation energies of some possible dissociation channels to produce those fragment ions were determined after the IE of $C_5H_{10}O$ and the AEs of nine fragment ions were obtained from their photoionization efficiency curves. The experimental dissociation energies of the simple bond cleavage reactions to form $C_5H_9^+$, $C_4H_7O^+$, and $C_3H_7O^+$ were in agreement with those predicted by G3B3 method. The formation processes for $C_4H_5^+$, $C_3H_5^+$, $C_3H_6O^+$, $C_2H_3O^+$, CH_3O^+, and $C_3H_7^+$ could involve transition states and intermediates. The reaction barriers V(G3B3) for $C_4H_5^+$ and $C_3H_5^+$ were respectively 2.98 eV and 3.53eV, which are in good agreement with their experimental dissociation energies.

The authors gratefully acknowledge the many valuable suggestions made by Professor Juguang Han (University of Science and Technology of China).

References

[1] SIDS initial assessment report for SIAM 4 [R]. Ispra, Italy, UNEP Publications, 1995: 23-25.

[2] Baker B, Guenther A, Greenberg J, et al. Canopy fluxes of 2-methyl-3-buten-2-ol over a ponderosa pine forest by relaxed eddy accumulation: Field data and model comparison [J]. Journal of Geophysical Research, 1999, 104: 26107-26114.

[3] Schade G W, Goldstein A H, Gray D W, et al. Canopy and leaf level 2-methyl-3-buten-2-ol fluxes from a ponderosa pine plantation [J]. Atmospheric Environment, 2000, 34: 3535-3544.

[4] Chan W H, Galloway M M, Kwan A J, et al. Photooxidation of 2-Methyl-3-buten-2-ol (MBO) as a potential source of secondary organic aerosol [J]. Environmental Science and Technology, 2009, 43: 4647-4652.

[5] Fantechi G, Jensen N R, Hjorth J, et al. Mechanistic studies of the atmospheric oxidation of methyl butenol by OH radicals, ozone and NO_3 radicals [J]. Atmospheric Environment, 1998, 32: 3547-3566.

[6] Atkinson R, Arey J. Gas-phase tropospheric chemistry of biogenic volatile organic compounds: a review [J]. Atmospheric Environment, 2003, 37: 197-219.

[7] Carrasco N, Doussin J F, O'Connor M, et al. Simulation chamber studies of the atmospheric oxidation of 2-Methyl-3-Buten-2-ol: reaction with Hydroxyl Radicals and Ozone under a variety of conditions [J]. Journal of Atmospheric Chemistry, 2007, 56: 33-55.

[8] Steiner A L, Tonse S, Cohen R C, et al. Biogenic 2-methyl-3-buten-2-ol increases regional ozone and HO_x sources [J]. Geophysical Research Letters, 2007, 34:15806(1-6).

[9] Vajda J H, Harrison A G. Proton affinities of some olefinic carbonyl compounds and heats of formation of $C_nH_{2n-1}O^+$ ions [J]. International Journal of Mass Spectrometry and Ion Physics, 1979, 30: 293-306.

[10] Zwinselman J J, Nibbering N M, Middlemiss N E, et al. A field Ionization kinetics and metastable ion study of the fragmentation of some pentenols [J]. Journal of Geophysical Research, 1981, 38: 163-179.

[11] Rudich Y, Talukdar R, Burkholder J B, et al. Reaction of methylbutenol with Hydroxyl radical: mechanism and atmospheric implications [J]. Journal of Physical Chemistry, 1995, 99: 12188-12194.

[12] Curtiss L A, Raghavachari K, Redfern P C, et al. Gaussian-3 (G3) theory for molecules containing first and second-row atoms [J].

Journal of Chemical Physics, 1998, 109: 7764-7776.

[13] Baboul A G, Curtiss L A, Redfern P C, et al. Gaussian-3 theory using density functional geometries and zero-point energies [J]. Journal of Chemical Physics, 1999, 110: 7650-7657.

[14] Frisch M J, Trucks G W, Schlegel H B, et al. Gaussian 03, Revision C.01 [EB/OL]. [2010-05-04]. http://www.psc.edu/general/software/packages/gaussian/G03C01_release_notes.html. Gaussian: Wallingford, CT, 2004.

[15] Wang S S, Kong R H, Shan X B, et al. Performance of the atomic and molecular physics beamline at the National Synchrotron Radiation Laboratory [J]. Journal of Synchrotron Radiation, 2006, 13: 415-420.

[16] Kong R H, Shan X B, Wang S S, et al. Experimental and theoretical study of Ne…CO cluster [J]. Journal of Electron Spectroscopy and Related Phenomena, 2007, 160: 49-53.

[17] Levy M, Yang W, Parr R G. A new functional with homogeneous coordinate scaling in density functional theory [J]. Journal of Chemical Physics, 1985, 83: 2334-2336.

[18] Kohn W, Becke A D, Parr R G. Density functional theory of electronic structure [J]. Journal of Physical Chemistry, 1996, 100: 12974-12980.

[19] Chiang S Y, Bahou M, Sankaran K, et al. Dissociative photoionization of CH_2Cl_2 and enthalpy of formation of $CHCl^+$: experiments and calculations [J]. Journal of Chemical Physics, 2003, 62: 118-125.

[20] Wang Z Y, Hao L Q, Zhou S K, et al. VUV dissociative photoionization of CHF_2Cl [J]. Journal of Molecular Structure, 2007, 826: 192-197.

[21] NIST. 3-Buten-2-01, 2-methyl- [S/OL]. [2010-05-04]. http://webbook.nist.gov/cgi/cbook.cgi? ID = C115184&Units = SI&Mask = 2A0.

甲基丁烯醇的光电离实验与理论研究

孙 月[1], 赵玉杰[1], 方文正[1], 孙金大[1], 单晓斌[1], 刘付轶[1], 盛六四[1], 王振亚[1,2]

(1 中国科学技术大学国家同步辐射实验室, 核科学技术学院, 合肥 230029;
2 中国科学院安徽光学精密机械研究所环境光谱学实验室, 合肥 230031)

摘 要 利用同步辐射光电离质谱的方法研究了甲基丁烯醇($C_5H_{10}O$)在 9.0 ~ 15.5eV 的真空紫外光电离和光解离过程. 通过测量光电离效率曲线, 得到了 $C_5H_{10}O$ 的电离能和主要碎片离子的出现势. 通过对实验和计算结果的比较, 分析了母体离子可能的光电离解离机理. 母体离子的解离通道可以分为 2 类: 由 $C_5H_{10}O^+$ 直接发生键断裂的解离和经由过渡态的解离. 确定了 $C_4H_5^+$ 和 $C_3H_5^+$ 离子的过渡态和中间体, 其反应势垒与实验解离能是符合的.

关键词 甲基丁烯醇, 光电离和光解离, 同步辐射, G3B3 计算